Table 1. Constants in the exchange factor correlation

	Specular	Diffuse
a_1	0.5711	0.5756
a_2	1.4704	1.5353
a_3	0.8237	0.8011
a_4	0.2079	0.1843

$\varepsilon_r = 0.35$ (specular surfaces) and from 0.94 to 0.97 for $\varepsilon_r = 0.85$ (diffuse surfaces). In practical packed beds, the porosity ranges between 0.3 and 0.6 with a value of 0.4 for randomly arranged, loosely packed monosized spheres. Therefore, the sensitivity of the radiant conductivity with respect to the porosity (as compared to other parameters) is not expected to be very significant.

REFERENCES

1. D. Vortmeyer, Radiation in packed solids, *Proceedings of 6th International Heat Transfer Conference*, Toronto, Vol. 6, pp. 525–539 (1978).
2. C.-L. Tien and B. L. Drolen, Thermal radiation in particulate media with dependent and independent scattering, *Ann. Rev. Num. Fluid Mech. Heat Transfer* **1**, 1–32 (1987).
3. M. Kaviany and B. P. Singh, Radiative heat transfer in porous media, *Adv. Heat Transfer* **23**, 133–186 (1993).
4. B. P. Singh and M. Kaviany, Independent theory versus direct simulation of radiative heat transfer in packed beds, *Int. J. Heat Mass Transfer* **34**, 2869–2881 (1991).
5. B. P. Singh and M. Kaviany, Modeling radiative heat transfer in packed beds, *Int. J. Heat Mass Transfer* **35**, 1397–1405 (1992).
6. C. K. Chan and C.-L. Tien, Radiative transfer in packed spheres, *ASME J. Heat Transfer* **96**, 52–58 (1974).
7. Y. S. Yang, J. R. Howell and D. E. Klein, Radiative heat transfer through a randomly packed bed of spheres by the Monte Carlo method, *ASME J. Heat Transfer* **105**, 325–332 (1983).
8. J. C. Chen and S. W. Churchill, Radiant heat transfer in packed beds, *A.I.Ch.E. Jl* **9**, 35–41 (1963).
9. M. Kaviany, *Principles of Heat Transfer in Porous Media*. Springer-Verlag, New York (1991).
10. S. V. Patankar, *Numerical Heat Transfer and Fluid Flow*. Hemisphere, Washington, DC (1980).

Pergamon

Int. J. Heat Mass Transfer. Vol. 37, No. 16, pp. 2583–2587, 1994

0017-9310/94 $7.00+0.00

Visualization of density fields in liquid metals

R. E. POOL and J. N. KOSTER†
Dept. of Aerospace Engineering Sciences, University of Colorado, Boulder, CO 80309-0429, U.S.A.

(*Received* 13 *December* 1993 *and in final form* 4 *March* 1994)

1. INTRODUCTION

THE EXPERIMENTAL study of liquid metal flows is required to better understand the physics of convective fluid flow and heat transfer in materials science applications. Improvement of the quality of electronic solids through control of the convective melt environment requires a thorough grasp of both buoyant and thermocapillary flow mechanisms in low Prandtl number fluids. A large number of convective studies towards this application have been made using high Prandtl number transparent fluids. However, due to the large difference in Prandtl number between transparent fluids and liquid metals, the driving mechanisms for convective flow have a different character. This was presented by, among others, Carpenter and Homsy [1], who showed large differences in surface tension gradients for high Prandtl number fluids vs low Prandtl number fluids. Knowledge of these low Prandtl number flow mechanisms will foster an improved understanding of materials solidification issues.

Because liquid metals are opaque, their study requires the use of unconventional flow analysis techniques. Historically, this has been limited to probing with thermocouples and observations of surface motion [2–4]. Also, highly intrusive electromagnetic techniques were used [5]. A new, non-invasive method of liquid metal flow visualization has recently been developed. The system described here uses real time radioscopy and has been employed with much success to visualize the melting and solidification interfaces [6–8]. The method has now been improved to permit coarse visualization of the density fields in liquid gallium. Analysis of the density fields can yield information concerning the character of the convective flow field as well as the nature of the heat transfer taking place. Real time visualization of the thermal fields is complementary to thermocouple probing because it allows visualization of the entire flow field. In addition, this method is non-intrusive and can be utilized for the visualization of multiple liquid layers where thermocouple techniques would interfere with the interface behavior.

To assess the heat transfer characteristics in a liquid metal it is desirable to have knowledge of the thermal fields within the fluid, especially during convective or unsteady flow. Creating isothermal patterns from convective fluids using the method of holographic interferometry [9] has proven to be useful for determining the character of convective flow. Not only is the temperature field clearly diagrammed, but also

†To whom correspondence should be addressed.

NOMENCLATURE

AR	aspect ratio, height/length	(μ/ρ)	linear absorption coefficient [cm^2 g^{-1}]
d	material thickness [cm]	ρ	fluid density [g cm^{-3}].
I	intensity		
T	temperature [K].		

Greek symbols

Δ	difference
Λ	temperature dependence of density [g cm^{-3} K^{-1}]

Subscripts

A	hot side
B	cold side
0	incident.

the direction and magnitude of the flow, as well as flow oscillations. These types of whole field observations are not easily made using temperature probing techniques.

The work by Campbell and Koster [8] showed that the 3% density difference between solid and liquid gallium could be clearly visualized, especially with the appropriate image processing techniques. When a fluid is differentially heated, the density of the fluid varies as a function of temperature. Since X-ray absorption is a function of material density, it was proposed that the difference in absorption from the hot and cold liquids could provide sufficient variation in intensity levels to be detected by the radioscopic image processing system. The governing equation for X-ray absorption in a particular material is given by:

$$I = I_0 \, e^{-(\mu/\rho)\rho d}, \tag{1}$$

where I is the resultant intensity, I_0 the initial intensity, (μ/ρ) the linear absorption coefficient, ρ the fluid density and d the material thickness in the direction of the penetrating radiation [10]. Given a differentially heated rectangular cavity (Fig. 1) with the hot side associated with the subscript A and the cold side associated with the subscript B, and recalling that the cavity thickness and linear absorption coefficient are constant on both sides, the ratio of intensities from the cold side to the hot side becomes:

$$\frac{I_B}{I_A} = e^{-((\mu/\rho)(\rho_B - \rho_A)d)}. \tag{2}$$

The temperature dependence $(-\partial\rho/\partial T)$ of a material is given by the variable $-\Lambda$, which for gallium is given as 0.56×10^{-3} g cm^{-3} K^{-1} [11]. Λ is assumed constant in the considered temperature range. Substituting this parameter in place of the density terms and accounting for the temperature difference, ΔT, equation (2) yields:

$$\frac{I_B}{I_A} = e^{-((\mu/\rho)(-\Lambda\,\Delta T)d}. \tag{3}$$

The percent density difference which must be detected for visualization of constant density fields in liquid gallium with an applied temperature difference of 8°C is calculated to be about $\Delta\rho = 0.2\%$. The equations above also implicate that this method is an integrating density measurement, similar to interferometric techniques, which precludes the visualization of three-dimensional effects.

EXPERIMENTAL SET-UP

The experimental facility consists of an X-ray system and an imaging system. The X-ray system is a standard NDT

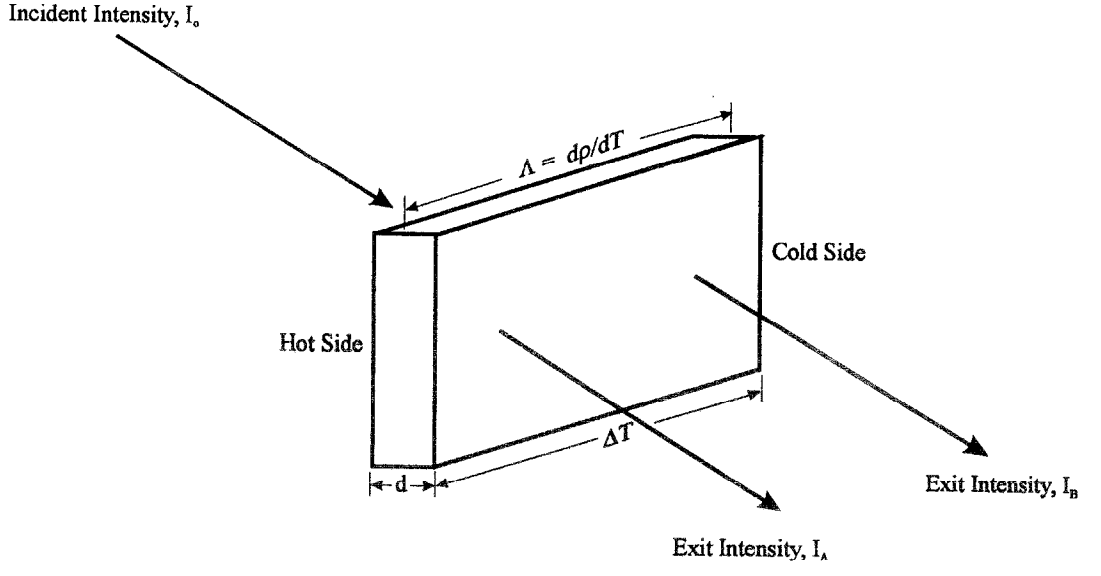

FIG. 1. Diagram illustrating variable absorption through a differentially heated cavity.

FIG. 2. Visualization of density fields in liquid gallium. The hot liquid is color coded in red.

facility manufactured by Ball Industrial Systems. It includes a 160 kV tungsten X-ray source which has a spot size of 0.4 mm × 0.4 mm. The X-rays are imaged on a CsI fluoroscopic screen and subsequently recorded via a CCD camera. The image is then transferred to a Hamamatsu DVS-3000 real time image processor. The processor is capable of background subtraction, time integration, and contrast and brightness adjustments. In addition, it has an image capture card which allows selected images to be transferred, via a GPIB connection, to a personal computer for additional image processing, such as enhancement and false coloring.

The test apparatus used for these experiments is the same as that used by Campbell and Koster [8] and will only be briefly described here. The gallium is contained in a plexiglas test cell with 1.25-cm-thick walls to provide adequate insulation. Heating of the side walls is accomplished via molybdenum-coated copper thermodes which exchange heat with the fluid from two recirculating thermostats. Temperature measurements are made using type K thermocouples inserted through the test cell lid. The amount of scattered radiation is limited through the use of a radiation precollimator, lead test cell masks and an X-ray criss-cross focal grid with 103 lines/inch.

Isothermalization of the gallium was done at around 50 C for a minimum of 3 h. Typical final temperature variations were ±0.2 C at the isothermal condition. After the background image was captured, the thermostats were ramped to achieve a high temperature gradient. Establishing a temperature gradient in the liquid gallium larger than about 8 C proved to be difficult due to heat loss in the system and the large thermal conductivity of the gallium.

RESULTS

The density fields visualized using this method are shown in Fig. 2. The image has been processed and color-coded using PhotoPaint™ software. The red region represents the hot liquid. The gallium was allowed to partially solidify to help read the image by indicating the direction of the temperature gradient. In addition, the shape of the solid–liquid interface verifies the direction of the convective flow and gives some indication of its intensity [8]. Three zones of varying temperature are discernible. The indication from this figure is that regions of different temperature fluid can be visualized in a liquid metal flow using radioscopic methods. These flow patterns can be compared to the numerical works of Kuo [12] and of Viswanath [13]. The experimental work of Stewart [3] using T/C probes also shows similar convective patterns. The Grashof number of the experiment was determined to be 4.3×10^6.

The radioscopic image (Fig. 2) discloses the current limiting resolution of this visualization technique. It is believed that the resolution is a composite problem arising from both the X-ray source size and the sensitivity and quantum physics of the fluoroscopic screen. This quantum mottle comes from the transformation process of X-rays into visible light in the CsI screen. Because the intensity variations are so small between the light transmitted through the hot and cold fluid, the differences which are discerned fall within the scintillation noise level of the CsI screen. In other words, the light response of the screen to variations in X-ray intensity is not presently adequate to differentiate the varying incident intensities with high clarity. The other source of noise and mottle comes from the target of the X-ray source. The shape of the Gaussian X-radiation emission distribution of the source target may also be a contributor [14]. In addition, a small degree of image unsharpness is created when the X-ray target has a finite size. The smaller the target size, the lower the degree of unsharpness [15]. Other parameters which can affect the image clarity, such as the distance from the liquid layer to the imaging screen and the distance from the liquid layer to the X-ray source, have been optimized to within the physical limits of the facility.

CONCLUSION

Visualization of density fields in liquid gallium has been successfully demonstrated. However, due to the large degree of quantum mottle present in the image, no more than three regions of similar density fluid were able to be discerned. This resolution provides a general indication of the behavior of the convective fluid, but is as yet insufficient for providing valuable quantitative data. It is believed, however, that, with further hardware improvements and the proper post-processing and image enhancement techniques, the images can be smoothed out to provide valuable real time visualization of convective flow patterns in liquid metals.

Acknowledgements—The research support from the NSF under CTS-8906846 and CTS-9114775 is greatly appreciated. The study also benefited from NASA support under NCC3-210. We appreciate the valuable discussions with T. Campbell.

REFERENCES

1. B. M. Carpenter and G. M. Homsy, Combined buoyant–thermocapillary flow in a cavity, *J. Fluid Mech.* **207,** 121–132 (1989).
2. D. Camel, P. Tinson and J. J. Favier, Marangoni flow regimes in liquid metals, *Acta Astronaut.* **13,** 723–726 (1986).
3. M. J. Stewart and F. Weinberg, Fluid flow in liquid metals. II. Experimental observations, *J. Crystal Growth* **12,** 228–238 (1971).
4. T. M. Wang, S. A. Korpela, M. C. Hung and C. D. Anderek, Convection in a shallow cavity. In *Numerical Simulation of Oscillatory Convection in Low-Pr Fluids, A GAMM Workshop* (Edited by B. Roux), pp. 344–353. Vieweg (1990).
5. R. Ricou and C. Vives, Local velocity and mass transfer measurements in molten metals using an incorporated magnet probe, *Int. J. Heat Mass Transfer* **25,** 1579–1588 (1982).
6. P. G. Barber, R. K. Crouch, A. L. Fripp, W. J. Debnam, R. F. Berry and R. Simchick, A procedure to visualize the melt–solid interface in Bridgman grown germanium and PbSnTl, *J. Crystal Growth* **74,** 228–230 (1986).
7. K. Kakimoto, M. Eguchi, H. Watanabe and T. Hibiya, *In-situ* observation of solid–liquid interface shape by X-ray radiography during silicon single crystal growth, *J. Crystal Growth* **91,** 509–514 (1988).
8. T. A. Campbell and J. N. Koster, Visualization of liquid/solid interface morphologies in gallium subject to natural convection, *J. Crystal Growth* (submitted).
9. J. N. Koster and U. Müller, Oscillatory convection in vertical slots, *J. Fluid Mech.* **139,** 363–390 (1984).
10. P. K. Klug and L. E. Alexander, *X-ray Diffraction Procedures*, pp. 78–103. Wiley, New York (1962).
11. T. Iida and R. I. L. Guthrie, *The Physical Properties of Liquid Metals*, p. 71. Clarendon Press, Oxford (1988).
12. H. P. Kuo and S. A. Korpela, Stability and finite amplitude natural convection in a shallow cavity with insulated top and bottom and heated from the side, *Physics Fluids* **31,** 33–42 (1988).
13. R. Viswanath and Y. Jaluria, Numerical simulation of phase change problems in enclosures: a comparison of different approaches, *Heat Transfer in Phase Change* **ASME HTD-205,** 55–62 (1992).
14. M. Purschko and M. Schaefer, Radiometric determination and graphical interpretation for the effective focal spots of X-ray tubes, Rich. Seifert & Co., Röntgenwerke, Comet Ltd., Personal communication (1993).
15. P. McIntire (Editor), *Nondestructive Testing Handbook* (2nd edn), Vol. 3, *Radiography and Radiation Testing*. American Society for Nondestructive Testing (1985).